

Thermal Resistance of Transferred-Silicon-Nanomembrane Interfaces

D. P. Schroeder,¹ Z. Aksamija,² A. Rath,¹ P. M. Voyles,¹ M. G. Lagally,¹ and M. A. Eriksson¹

¹*University of Wisconsin-Madison, Madison, Wisconsin 53706, USA*

²*University of Massachusetts-Amherst, Amherst, Massachusetts 01003, USA*

(Received 30 April 2015; revised manuscript received 17 September 2015; published 15 December 2015)

We report measurements of the interfacial thermal resistance between mechanically joined single crystals of silicon, the results of which are up to a factor of 5 times lower than any previously reported thermal resistances of mechanically created interfaces. Detailed characterization of the interfaces is presented, as well as a theoretical model incorporating the critical properties determining the interfacial thermal resistance in the experiments. The results demonstrate that van der Waals interfaces can have very low thermal resistance, with important implications for membrane-based micro- and nanoelectronics.

DOI: 10.1103/PhysRevLett.115.256101

PACS numbers: 68.35.bg, 68.35.Ct, 68.35.Ja

Nanoscale thermal management is of fundamental importance in modern electronics [1,2], and as electronic device dimensions continue to shrink, thermal transport becomes increasingly dominated by structural interfaces and materials inhomogeneities [3]. For applications, either low or high thermal resistance may be important. The former is critical, e.g., for mitigating the effects of hotspots [4], while the latter is important for thermoelectric energy conversion applications [5,6]. It thus is important to be able to fabricate, grow, or assemble structures that reach either limit. With the advent of transferable and flexible electronics based on semiconductor membranes—which frequently involve composites of quite disparate materials—the question of thermal transport across interfaces is becoming increasingly important [7–9].

In this Letter, we present measurements of the thermal resistance of a simple, model interface that is also important for applications: a thin crystalline-silicon sheet transferred and bonded to a silicon substrate. This experiment enables us to extract the interfacial thermal resistance (ITR) between two well-aligned, identical, single crystals. Because the crystals have no acoustic mismatch, the nature of the interface itself is paramount in determining the ITR. We show that these transferred Si-Si interfaces can have an ITR as low as 2.8 m²K/GW. Further, we demonstrate that the surface condition is critical in determining and controlling the thermal resistance across the interface through modulation of the interfacial bonding energy. Interfaces formed between Si surfaces that are hydrogen terminated have an ITR of 9.2 m²K/GW, more than 3 times higher than that observed when one of the surfaces is terminated by a thin oxide layer. Both values are lower than any previously reported ITR of mechanically joined interfaces [10–14]. We support the thermal measurements with characterization of the interfaces by high-resolution scanning transmission electron microscopy (STEM) and atomic force microscopy (AFM). We present theoretical calculations of the ITR using a modification of the acoustic

mismatch model [15] and a theoretical framework for van der Waals (vdW) bonded interfaces [16]. The theory shows that the experimental results can be explained in terms of two parameters, interface separation and interfacial bonding energy, offering a simple framework for understanding thermal resistance in transferred membranes and interfaces.

Individual materials interfaces are both the real and conceptual building blocks of larger systems, yet in spite of the critically important role interfaces play, the majority of previous ITR measurements have focused on only a single type of interface: that between a metal film deposited on a nonmetal substrate, which lends itself to measurement by thermorefectance [3]. Such metal-nonmetal interfaces typically have a low ITR, with almost all values reported between 2.2 and 20 m²K/GW [10,12,17–39]. High-quality epitaxial interfaces, such as those between TiN and MgO, have been shown to have an even lower ITR of 1.4 m²K/GW [40]. Recently, it has become possible to measure the ITR of mechanically joined interfaces, and measurements of such interfaces have yielded larger ITR values, from 15 to 110 m²K/GW [10–14]. While the membrane transfer process allows the creation of interfaces between single-crystal Si and essentially arbitrary substrates, it is an open question whether such interfaces, formed by mechanical transfer, can exhibit a low ITR. We show here that such interfaces can have an ITR as low or lower than metal films deposited (e.g., evaporated or sputtered) on dielectrics.

The samples we study are fabricated by transfer printing (100)-oriented Si nanomembranes (NMs) onto bulk (100) Si substrates using the thermal-release tape method [41]. Because we measure 14 different samples, each with up to eight different membranes, care is taken to align the crystal axes of each Si nanomembrane to the underlying substrate, primarily to ensure that the interfaces formed beneath all of the transferred membranes are as similar as possible to each other. Although the effects of acoustic mismatch are expected to be small (as discussed below), the good

crystalline alignment has the added benefit that there is no acoustic mismatch across the interface, enabling us to focus on the influence of the interface itself. Repeating the transfer process, we can stack two membranes on top of each other, producing two Si-Si vdW-bonded interfaces in series, and enabling a check for consistency with the results obtained from single interfaces. Because the NMs are only 300 nm thick, the interfaces are close to the outer, instrument accessible surface, enabling high-resolution measurement of the ITR, which is otherwise obscured by a large bulk signal. After transfer, the highest temperature the interfaces experience during processing is 300 °C, as described in Ref. [42].

Figure 1 shows the two interface configurations we study here: in the upper diagrams of Figs. 1(a) and 1(c), interfaces are formed between a pair of H-terminated Si surfaces (H-H interface), and in the lower two diagrams, interfaces are formed between a H-terminated surface and an oxide-terminated surface (H-ox interface). Hydrogen terminated surfaces are achieved in a hydrofluoric acid bath, while oxide terminated surfaces are created in a piranha solution [45]. Because the interface (or interfaces) of interest are much closer to the surface than the width of the patterned metal thin film on the surface, the ITR can be determined by subtracting the results of 3ω measurements [46] performed with and without the interface of interest, enabling the isolation of the thermal resistance arising from the interface(s) under study [42].

Figure 1(b) shows the differential thermal resistance results for many single- and double-interface H-H and H-ox samples. Each marker represents a differential measurement, as described in Ref. [42]. The mean value of the

resistance for each type of sample is given by the solid line: brown for the H-H samples, and blue for the H-ox samples. The shading represents 1 standard deviation for each sample type. For both interface types, the samples with two interfaces in series are twice as resistive as the samples with a single interface within experimental uncertainty. From the values of thermal resistance through single- and double-interface structures, we determine the ITR of a single H-H interface between two well-aligned Si(100) regions to be $9.2 \pm 2.3 \text{ m}^2\text{K/GW}$, and of a single H-ox interface between the same two regions to be $2.8 \pm 0.9 \text{ m}^2\text{K/GW}$.

In order to understand the phonon transport through the vdW-bonded H-H and H-ox interfaces, it is important to consider their thickness, roughness, and bonding energy. To measure the total thickness of the interfacial region, scanning transmission electron microscopy is performed on both H-H and H-ox type samples. Electron transparent cross-sectional TEM samples are prepared directly on a previously measured four-probe measurement device via an *in situ* lift-out technique that uses focused-ion-beam etching.

Figure 2 shows high-resolution STEM images of the interface region for both sample types. The average H-H interface thickness is 1.5 nm, while the average H-ox interface thickness is 2.9 nm. These thicknesses represent the total distance between Si crystals, which is larger than the separation distance of the vdW-bonded interface, as schematically illustrated in Fig. 2(c), because each Si surface has a covalently bonded termination, which is not visible by STEM. It is the distance of these surface terminations from each other that defines the thickness of the vdW-bonded interface separation, for which the STEM results provide a definitive upper bound.

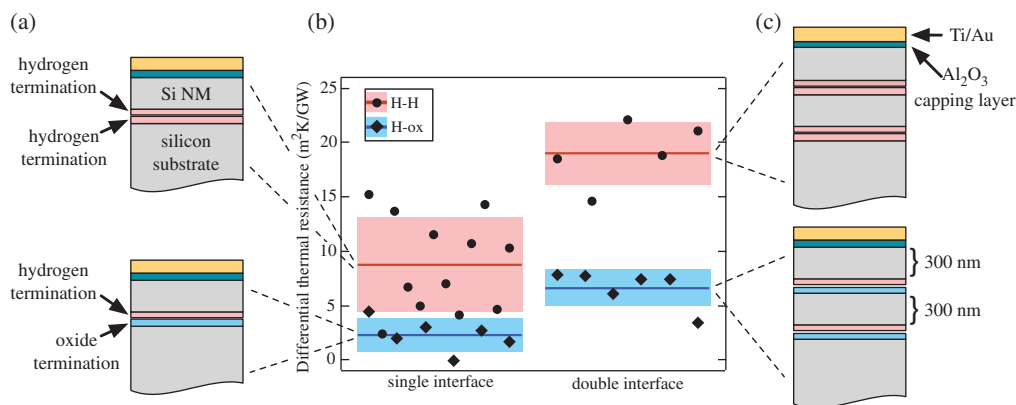


FIG. 1 (color). Schematic device cross sections and corresponding thermal resistance results. (a) Schematic device cross sections of single-interface H-H and H-ox devices, not to scale. Silicon nanomembranes are mechanically transferred onto bulk silicon receiver substrates. After transfer, the samples are capped with a layer of Al_2O_3 , and Ti/Au microstructures are fabricated on top. We create two types of devices—those in which the receiving surface is hydrogen terminated, and those in which the receiving surface is oxide terminated. In all cases the undersides of the NMs are hydrogen terminated. (b) Differential thermal resistance values of single- and double-interface nanomembrane sample structures. H-H interface values are given by circles, H-ox values by diamonds. Each marker represents a single independent measurement run. The mean value of each type of sample is given by the solid line; the standard deviation is given by the shaded region. For both interface types, the samples with two interfaces are twice as resistive as the samples with a single interface. (c) Schematic device cross sections of double interface H-H and H-ox devices. Double interface samples are fabricated by the same method as single interface samples, with the surface preparation and NM transfer iterated twice.

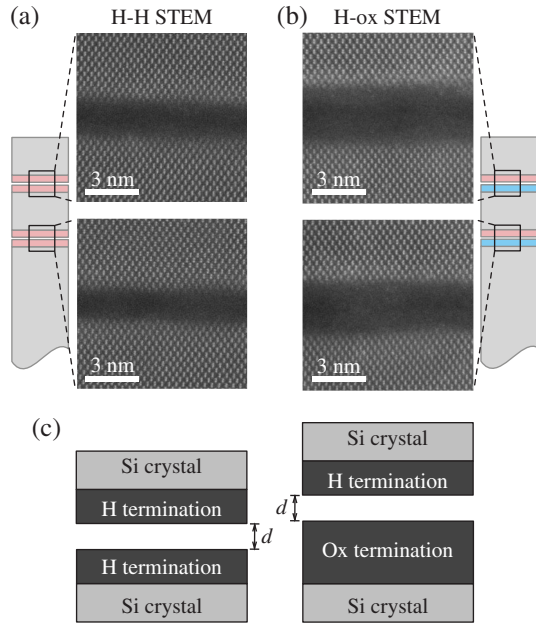


FIG. 2 (color). High-resolution z -contrast STEM images of typical H-H and H-ox interfaces taken along the $[110]$ zone axis of Si, used for interface characterization. (a) The H-H interfaces have a total interfacial thickness of 1.5 nm. (b) The presence of an additional oxide layer at the H-ox interfaces increases the total thickness to 2.9 nm. (c) Schematic diagram of the interface for both H-H and H-ox type samples. The total interface thickness is greater than the interfacial separation distance d because each surface has a termination that is not visible by STEM.

The rotational alignment of the membrane transfer, also important to our understanding of phonon transport through the interface, is very good in all samples measured by STEM. As can be seen by the well-aligned Si dumbbells in the silicon regions on either side of the interface, the rotational alignment is within 1° [47].

To determine the interface roughness, which is difficult to estimate by STEM, AFM measurements were conducted. Measurements were taken on four surfaces: H-terminated and oxide-terminated receiver substrates as prepared for NM transfer, the exposed top NM surface directly after transfer, and the exposed substrate adjacent to that membrane after transfer. The roughness is consistent across all measured surfaces, with an average root-mean-square (rms) roughness of 0.12 nm and an average peak-to-peak roughness of 1.1 nm. Because all measured roughnesses were consistent, regardless of what processing steps each surface had been exposed to, we assume that the bottom surface of the NM, at the interface, has this same roughness.

Also key to modeling the ITR is the bonding energy of each interface, which is available from previous wafer bonding experiments. The H-H interface bonding energy has been measured to be 30 mJ/m^2 at room temperature, and 100 mJ/m^2 after annealing to 300°C [48]. H-ox

bonding has been shown to be $60\text{--}80 \text{ mJ/m}^2$ at room temperature with no anneal [49]. While to our knowledge the bonding energy of such H-ox interfaces annealed to a temperature of 300°C has not been previously published, the presence of OH groups is known to enable increases in bonding strength at lower temperatures than for surfaces that lack such groups [50].

We use these results in a model that we refer to here as the vdW-AMM model and that is based on the acoustic mismatch model (AMM) [15] and the theory of thermal conduction through van der Waals bonded interfaces [16]. To model thermal transport through an interface, it is important to know the transmission coefficient τ for each phonon mode \vec{q} . Within the vdW-AMM model, the phonon transmission coefficient $\tau_b^{\text{vdW}}(\vec{q})$ due to the vdW contact between identical materials is

$$\tau_b^{\text{vdW}}(\vec{q}) = \frac{1}{1 + \frac{\omega_b^2(\vec{q})}{4K_A^2} Z_b^2(\vec{q}) \cos^2 \Theta}, \quad (1)$$

where $\omega_b(\vec{q})$ is the phonon angular frequency of mode \vec{q} on phonon branch b making an angle Θ with the interface normal, and $Z_b(\vec{q})$ is the acoustic impedance. K_A is the spring constant per unit area, and is dependent on the interfacial separation distance d and the interfacial energy γ [42].

Phonon transmission through interfaces generally does not get interrupted at low phonon frequencies, whereas phonons with higher frequencies experience more scattering, because their wavelength becomes comparable to the nanoscale size of interfacial imperfections. This feature can be observed directly in Eq. (1), where the phonon transmission through the vdW interface reaches unity as the phonon angular frequency ω goes to zero, corresponding to the acoustic or long wavelength limit, and as ω increases, the transmission decays as ω^{-2} .

The interface conductance σ^{vdW} is obtained from the transmission coefficient by summing over all phonon branches b that contribute to transport in each layer i , and all modes \vec{q} [51,52]:

$$\sigma_{i,T}^{\text{vdW}} = \frac{1}{2} \sum_{b,\vec{q}} \frac{C_{b,T}(\vec{q}) v_b(\vec{q}) \cos \Theta \tau_b^{\text{vdW}}(\vec{q})}{1 - \langle \tau_b^{\text{vdW}}(\vec{q}) \rangle}, \quad (2)$$

where $C_{b,T}(\vec{q})$ is the modal heat capacity given by

$$C_{b,T}(\vec{q}) = \frac{[\hbar \omega_b(\vec{q})]^2}{k_B T^2} \frac{e^{(\hbar \omega_b(\vec{q})/k_B T)}}{[e^{(\hbar \omega_b(\vec{q})/k_B T)} - 1]^2}, \quad (3)$$

and T is the temperature. The correction factor in the denominator of Eq. (2) ensures that the interface resistance goes to zero in the limit of a fictitious ideal interface between two identical materials, where τ^{vdW} becomes unity and the interface resistance must vanish [53].

The results of the vdW-AMM calculations are displayed in Fig. 3. The vdW-AMM component of the total ITR is plotted for both interface types as a function of both the interface separation distance d , on the vertical axis, and the interfacial bonding strength γ , on the horizontal axis.

Using the previously measured bonding strength for H-H interfaces of $\gamma = 100 \text{ mJ/m}^2$ [48] and our measured value for the H-H ITR of $9.2 \text{ m}^2\text{K/GW}$, the vdW-AMM model gives an interfacial separation distance of $d = 0.38 \text{ nm}$ (the blue circle in Fig. 3). This value describes the distance between vdW-bonded planes at the H-H interface, is smaller than the total separation distance between Si crystals, as expected, and is consistent with the roughness measurements performed on membrane and substrate surfaces.

Because the oxide-terminated and H-terminated surfaces have equal roughness, we assume the H-ox interfaces have interfacial separations equal to those of the H-H interfaces. The additional 1.4 nm of amorphous oxide termination at the H-ox interface contributes a thermal resistance in series with the vdW-bonded interface. We account for this by using the minimum-thermal-conductivity calculation for amorphous SiO_2 of $\kappa_{\text{ox}} = 1.05 \text{ W/(mK)}$ [54], which yields a resistance of $R_{\text{ox}} = 1.5 \text{ m}^2\text{K/GW}$. The total interfacial thermal resistance is then given by $\text{ITR} = R_{\text{ox}} + R_{\text{vdW}}$, yielding $R_{\text{vdW}} = 1.3 \text{ m}^2\text{K/GW}$ at the H-ox interface. Inverting the vdW-AMM model reveals the bonding strength of this interface to be $\gamma = 300 \text{ mJ/m}^2$ (the red circle in Fig. 3). This result is consistent with the expectation of increasing the bonding strength through annealing.

It is useful to compare the ITR of the H-ox interface with one of the common theoretical interfaces that can be regarded as a limit of van der Waals bonding: a hypothetical

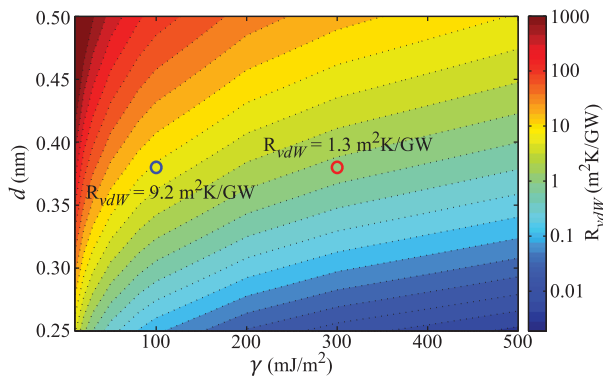


FIG. 3 (color). Contribution to the ITR due to vdW bonding as a function of the interfacial separation distance d and bonding strength γ , calculated from the vdW-AMM model. The thermal resistivity is dependent on the spring constant K_A , which is proportional to the adhesion energy γ [42]. Consequently, the ITR decreases with γ , approximately as $1/\gamma^2$, and it increases with d . The experimental thermal resistance results are shown, with the H-H (red circle) and H-ox (blue circle) interfaces both consistent with calculations at $d = 0.38 \text{ nm}$ and $\gamma = 100 \text{ mJ/m}^2$ and 300 mJ/m^2 , respectively.

perfect Si-Si interface that is limited by a single perfectly diffuse scattering layer. This type of interface, in which every phonon is scattered with uniform probability into a completely random direction, corresponds to the diffuse mismatch model [52], and calculations using this model for transmission from Si into Si yield an ITR of $0.61 \text{ m}^2\text{K/GW}$. The portion of the H-ox ITR that we attribute to the vdW bonding of the interface is only a factor of 2 larger than this result, emphasizing the extremely low thermal resistance achieved by those H-ox interfaces.

Using the vdW-AMM model, we also calculate the expected ITR of several related interface types. Si(111) membranes transferred to Si(100) substrates have a theoretical increase in the ITR of less than 10% over the results shown here for Si(100) transferred to Si(100). This provides an upper bound on the possible increase in the ITR due to crystallographic mismatch, including rotational misalignment. In addition, we have done calculations of interfaces between Sn crystals, heavier than Si, given the same interfacial properties as the H-ox Si-Si system. We find that the vdW contribution to the ITR rises to $1.9 \text{ m}^2\text{K/GW}$. This increase in thermal resistance is driven by the reduced phonon group velocity in Sn, leading to fewer phonons incident on the interface. The opposite effect will be true for lighter materials, such as diamond. The calculations for Sn-Sn and Si(111)-Si(100) interfaces show that, even with changes in materials properties and phonon dispersions, the ITR values we measure here are comparable with expectations for van der Waals interfaces for other materials, and thus the interface itself contributes essentially to the thermal transport.

Previous studies have suggested that the presence of an oxide at a mechanically created Si-Si interface has a negligible effect on interfacial thermal resistance [14]. We see here, however, that the oxide contribution to the thermal resistance is only negligible for interfaces with high overall thermal resistance, such as unannealed samples. More importantly, however, we see that even if the resistance of the oxide itself is negligible, the role the oxide plays in the bonding strength of the interface is vital. Further, past studies have compared the ITR between interfaces fabricated on H-terminated substrates to that between interfaces fabricated on oxide-terminated substrates, although not in Si-Si structures. The results of these studies have not been conclusive, with multiple reports of an increased ITR at the oxide interface [25,30], as well as multiple reports of the opposite effect, a decreased ITR at the oxide interface [22,24,33]. Here, we find clear evidence that oxide-terminated substrates lead to a lower ITR between mechanically joined single-crystal silicon regions due to the increased interfacial bonding energy when compared to interfaces with hydrogen-terminated substrates.

In conclusion, we show that vdW-bonded interfaces of transferred nanomembranes can have very low

interfacial thermal resistance. Further, the surface condition of vdW-bonded interfaces between like materials can affect the ITR by over 300%: interfaces created by transfer printing hydrogen-terminated silicon nanomembranes onto oxide-terminated silicon receiver substrates show a significantly lower interfacial thermal resistance than those formed by transferring to hydrogen-terminated substrates because of increased interfacial bonding energy and despite additional oxide thermal resistance and a greater separation distance between Si crystals. The vdW-AMM model accurately captures and describes the interface-specific properties critical to the ITR and confirms our understanding of the experimental ITR values, characterization measurements, and theoretical modeling methods. We show the direct relationship between the ITR and bonding energy. The results are important for the future of thermal management in electronic devices built on flexible, stretchable, and transferable nanomembranes.

We thank Irena Knezevic and Gabriel Jaffe for useful discussions and comments on the manuscript and Arnold Kiefer for experimental assistance. This research was supported by DOE Grant No. DE-FG02-03ER46028, except for the electron microscopy experiments by A. R. and P. M. V., which were supported by DOE Grant No. DE-FG02-08ER46547.

-
- [1] E. Pop, *Nano Res.* **3**, 147 (2010).
 [2] H. Alam and S. Ramakrishna, *Nano Energy* **2**, 190 (2013).
 [3] D. G. Cahill, P. V. Braun, G. Chen, D. R. Clarke, S. Fan, K. E. Goodson, P. Keblinski, W. P. King, G. D. Mahan, A. Majumdar, H. J. Maris, S. R. Phillpot, E. Pop, and L. Shi, *Appl. Phys. Rev.* **1**, 011305 (2014).
 [4] A. Bar-Cohen and P. Wang, *J. Heat Transfer* **134**, 051017 (2012).
 [5] A. Majumdar, *Science* **303**, 777 (2004).
 [6] C. J. Vineis, A. Shakouri, A. Majumdar, and M. G. Kanatzidis, *Adv. Mater.* **22**, 3970 (2010).
 [7] J. A. Rogers, T. Someya, and Y. Huang, *Science* **327**, 1603 (2010).
 [8] F. Cavallo and M. G. Lagally, *Soft Matter* **6**, 439 (2010).
 [9] A. L. Moore and L. Shi, *Mater. Today* **17**, 163 (2014).
 [10] S. T. Huxtable, D. G. Cahill, and L. M. Phinney, *J. Appl. Phys.* **95**, 2102 (2004).
 [11] R. Y. Wang, R. A. Segalman, and A. Majumdar, *Appl. Phys. Lett.* **89**, 173113 (2006).
 [12] D.-W. Oh, S. Kim, J. A. Rogers, D. G. Cahill, and S. Sinha, *Adv. Mater.* **23**, 5028 (2011).
 [13] M. D. Losego, M. E. Grady, N. R. Sottos, D. G. Cahill, and P. V. Braun, *Nat. Mater.* **11**, 502 (2012).
 [14] D. Grimm, R. B. Wilson, B. Teshome, S. Gorantla, M. H. Rummeli, T. Bublat, E. Zallo, G. Li, D. G. Cahill, and O. G. Schmidt, *Nano Lett.* **14**, 2387 (2014).
 [15] Z. Aksamija and I. Knezevic, *Phys. Rev. B* **88**, 155318 (2013).
 [16] R. Prasher, *Appl. Phys. Lett.* **94**, 041905 (2009).
 [17] E. T. Swartz and R. O. Pohl, *Appl. Phys. Lett.* **51**, 2200 (1987).
 [18] R. J. Stoner and H. J. Maris, *Phys. Rev. B* **48**, 16373 (1993).
 [19] Y. Zhao, C. Zhu, S. Wang, J. Z. Tian, D. J. Yang, C. K. Chen, H. Cheng, and P. Hing, *J. Appl. Phys.* **96**, 4563 (2004).
 [20] B. C. Gundrum, D. G. Cahill, and R. S. Averback, *Phys. Rev. B* **72**, 245426 (2005).
 [21] R. J. Stevens, A. N. Smith, and P. M. Norris, *J. Heat Transfer* **127**, 315 (2005).
 [22] H.-K. Lyeo and D. G. Cahill, *Phys. Rev. B* **73**, 144301 (2006).
 [23] P. E. Hopkins, P. M. Norris, and R. J. Stevens, *J. Heat Transfer* **130**, 022401 (2008).
 [24] K. C. Collins, S. Chen, and G. Chen, *Appl. Phys. Lett.* **97**, 083102 (2010).
 [25] P. E. Hopkins, L. M. Phinney, J. R. Serrano, and T. E. Beechem, *Phys. Rev. B* **82**, 085307 (2010).
 [26] J. Reifenberg, K.-W. Chang, M. Panzer, S. Kim, J. Rowlette, M. Asheghi, H.-S. Wong, and K. Goodson, *IEEE Electron Device Lett.* **31**, 56 (2010).
 [27] Y. Xu, R. Kato, and M. Goto, *J. Appl. Phys.* **108**, 104317 (2010).
 [28] A. J. Minnich, J. A. Johnson, A. J. Schmidt, K. Esfarjani, M. S. Dresselhaus, K. A. Nelson, and G. Chen, *Phys. Rev. Lett.* **107**, 095901 (2011).
 [29] P. E. Hopkins, J. C. Duda, C. W. Petz, and J. A. Floro, *Phys. Rev. B* **84**, 035438 (2011).
 [30] W.-P. Hsieh, A. S. Lyons, E. Pop, P. Keblinski, and D. G. Cahill, *Phys. Rev. B* **84**, 184107 (2011).
 [31] J. C. Duda and P. E. Hopkins, *Appl. Phys. Lett.* **100**, 111602 (2012).
 [32] P. J. O'Brien, S. Shenogin, J. Liu, P. K. Chow, D. Laurencin, P. H. Mutin, M. Yamaguchi, P. Keblinski, and G. Ramanath, *Nat. Mater.* **12**, 118 (2013).
 [33] C. Monachon and L. Weber, *J. Appl. Phys.* **113**, 183504 (2013).
 [34] J. C. Duda, C.-Y. P. Yang, B. M. Foley, R. Cheaito, D. L. Medlin, R. E. Jones, and P. E. Hopkins, *Appl. Phys. Lett.* **102**, 081902 (2013).
 [35] E. Dechaumphai, D. Lu, J. J. Kan, J. Moon, E. E. Fullerton, Z. Liu, and R. Chen, *Nano Lett.* **14**, 2448 (2014).
 [36] C. S. Gorham, K. Hattar, R. Cheaito, J. C. Duda, J. T. Gaskins, T. E. Beechem, J. F. Ihlefeld, L. B. Biedermann, E. S. Piekos, D. L. Medlin, and P. E. Hopkins, *Phys. Rev. B* **90**, 024301 (2014).
 [37] R. B. Wilson and D. G. Cahill, *Nat. Commun.* **5**, 5075 (2014).
 [38] R. Cheaito, J. T. Gaskins, M. E. Caplan, B. F. Donovan, B. M. Foley, A. Giri, J. C. Duda, C. J. Szejewski, C. Constantin, H. J. Brown-shaklee, J. F. Ihlefeld, and P. E. Hopkins, *Phys. Rev. B* **91**, 035432 (2015).
 [39] R. B. Wilson, B. A. Apgar, W.-P. Hsieh, L. W. Martin, and D. G. Cahill, *Phys. Rev. B* **91**, 115414 (2015).
 [40] R. M. Costescu, M. A. Wall, and D. G. Cahill, *Phys. Rev. B* **67**, 054302 (2003).
 [41] A. M. Kiefer, D. M. Paskiewicz, A. M. Clausen, W. R. Buchwald, R. A. Soref, and M. G. Lagally, *ACS Nano* **5**, 1179 (2011).
 [42] See Supplemental Material at <http://link.aps.org/supplemental/10.1103/PhysRevLett.115.256101>, which

- includes Refs. [43] and [44], for further details on fabrication, measurement, characterization, and theoretical modeling.
- [43] W. Weber, *Phys. Rev. B* **15**, 4789 (1977).
- [44] Z. Aksamija and I. Knezevic, *Phys. Rev. B* **82**, 045319 (2010).
- [45] Y. J. Chabal and L. C. Feldman, *Interface* **14**, 31 (2005).
- [46] D. G. Cahill, M. Katiyar, and J. R. Abelson, *Phys. Rev. B* **50**, 6077 (1994).
- [47] Z. Yu, D. A. Muller, and J. Silcox, *Ultramicroscopy* **108**, 494 (2008).
- [48] Q.-Y. Tong, E. Schmidt, U. Gösele, and M. Reiche, *Appl. Phys. Lett.* **64**, 625 (1994).
- [49] K. Ljungberg, U. Jansson, S. Bengtsson, and A. Soderbärg, *J. Electrochem. Soc.* **143**, 1709 (1996).
- [50] U. Gösele, Y. Bluhm, G. Kästner, P. Kopperschmidt, G. Kräuter, R. Scholz, A. Schumacher, St. Senz, Q.-Y. Tong, L.-J. Huang, Y.-L. Chao, and T. H. Lee, *J. Vac. Sci. Technol. A* **17**, 1145 (1999).
- [51] S. Simons, *J. Phys. C* **7**, 4048 (1974).
- [52] E. T. Swartz and R. O. Pohl, *Rev. Mod. Phys.* **61**, 605 (1989).
- [53] G. Chen and T. Zeng, *Microscale Thermophys. Eng.* **5**, 107 (2001).
- [54] D. G. Cahill, S. K. Watson, and R. O. Pohl, *Phys. Rev. B* **46**, 6131 (1992).